

Original article

Understanding gas-enhanced methane recovery in graphene nanoslits via molecular simulations

Dias Bekeshov¹, Sultan Ashimov¹, Yanwei Wang^{1,2}^{*}, Lei Wang^{3,4}^{*}

¹Department of Chemical & Materials Engineering, School of Engineering and Digital Sciences, Nazarbayev University, Astana 010000, Kazakhstan

²Laboratory of Computational Materials Science, Center for Energy and Advanced Materials Science, National Laboratory Astana, Astana 010000, Kazakhstan

³State Key Laboratory of Oil and Gas Reservoir Geology and Exploitation, College of Energy, Chengdu University of Technology, Chengdu 610059, P. R. China

⁴Department of Petroleum Engineering, School of Mining and Geosciences, Nazarbayev University, Astana 010000, Kazakhstan

Keywords:

Shale gas
coalbed methane
adsorption
molecular dynamics
Monte Carlo simulation
carbon dioxide

Cited as:

Bekeshov, D., Ashimov, S., Wang, Y., Wang, L. Understanding gas-enhanced methane recovery in graphene nanoslits via molecular simulations. *Capillarity*, 2023, 6(1): 1-12.

<https://doi.org/10.46690/capi.2023.01.01>

Abstract:

Shale gas and coalbed methane are energy sources that mainly consist of methane stored in an adsorbed state in the pores of the organic-rich rock and coal seams. In this study, the graphene nanoslit model is employed to model the nanometer slit pores in shale and coal. Grand canonical Monte Carlo and molecular dynamics modeling methods are used to investigate the mechanisms of adsorption and displacement of methane in graphene-based nanoslit pores. It is found that as the width of the slit pore increases, the adsorption amount of gas molecules increases, and the number density profile of adsorbed methane molecules alters from monolayer to multilayer adsorption. The minimum slit pore width at which methane molecules can penetrate the slit pore is determined to be 0.7 nm. Moreover, it is demonstrated that by lowering the temperature, the adsorption rate of the methane increases since the adsorption is an exothermic process. Enhancing methane recovery was investigated by the injection of gases such as CO₂ and N₂ to displace the adsorbed methane. The comparison of adsorption isotherms of gas molecules provides the following order in terms of the amount of adsorption, CO₂ > CH₄ > N₂, for the same slit pore width and the same temperature and pressure conditions.

1. Introduction

Natural gas is a fossil energy resource formed deep beneath the earth's surface through millions of years of geochemical evolution. Natural gas could contain quite a few different gas compounds, in which methane (CH₄) is usually the dominant component. Compared to other fossil fuels, such as coal and crude oil, natural gas is a relatively clean energy resource. Based on the technological and economical difficulty involved in exploitation processes, natural gas resources can be classified into conventional and unconventional types, the latter of which nowadays attracts more and more attention provided the

increasing worldwide energy demand. Two major members of unconventional gas resources are shale gas and coal bed methane (CBM) (Asif et al., 2022; Qin et al., 2022).

Shale gas is an abundant unconventional gas resource that has been booming for almost two decades, thanks to the efficient implementation of horizontal drilling and multistage hydraulic fracturing (Caulton et al., 2014; Huai et al., 2020; Lyu et al., 2021; Qiao et al., 2022). Large amounts of methane stored in the shale matrix are existing in an adsorption state, especially in the organic nanopores (Loucks et al., 2009; Sharma et al., 2015). Methane adsorption not only affects the prediction of gas reserve estimation but also depresses the ef-

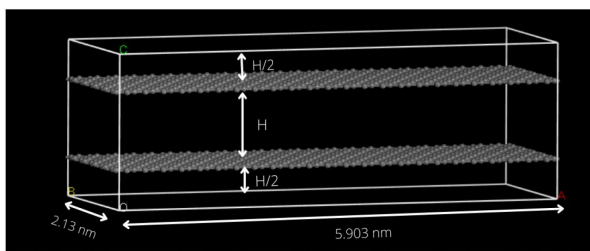


Fig. 1. Rectangular model of the nanoslit with the pore size 1 nm used in GCMC simulations.

efficiency of production. To improve shale gas and CBM recovery efficiency, gas injection to displace adsorbed methane and storage in both shale and coal formations has been investigated as a technical option with promising capacity (Wang et al., 2014; Liu et al., 2019; Shi et al., 2019; Lyu et al., 2021). Carbon dioxide (CO_2) alongside by nitrogen (N_2) could be used to displace CH_4 from the shale, the process known as enhanced shale gas recovery (ESGR) (Oudinot et al., 2017; Hu et al., 2019; Zheng et al., 2020). This allows to sequestrate CO_2 to mitigate anthropogenic greenhouse gas emissions (mostly CO_2), and help achieve net-zero CO_2 emissions by 2050 (Becattini et al., 2022). Therefore, it is important to study the competitive adsorption mechanisms of methane and injected gas as well as the displacement process in organic nanopores for the evaluation of recoverable gas reserves and efficient production of shale and CBM gas.

The adsorption behavior of methane in carbon-based nanostructures has been studied by a number of researchers (Kang et al., 2011; Tinni et al., 2012; Akkutlu and Fathi, 2012; Wu et al., 2015; Lin et al., 2017; Zhao et al., 2019; Baykasoglu et al., 2021; Cheng et al., 2021; Taheri and Pour, 2021; Xu et al., 2022). For instance, Wu et al. (2015) used molecular dynamics (MD) simulations to investigate the adsorption and displacement of CH_4 by CO_2 and N_2 in slit pores composed of graphite slabs and with pore sizes of 7 Å, 10 Å, 15 Å and 20 Å based on the “united atom” models. Lin et al. (2017) used both MD and Grand canonical Monte Carlo (GCMC) simulations to study the adsorption of methane at 300 K, 320 K, 340 K and 360 K, and the pressure range of 1 to 40 MPa, with pore sizes of 2 to 11 nm. They also found out that the methane adsorption energy on monolayer graphene is similar to the adsorption energy of shale. Therefore, graphene can be used to represent shale in molecular simulations. Zhao et al. (2019) performed GCMC simulations at pressures up to 40 MPa and fixed temperature of 333.15 K to investigate the adsorption behavior of methane in graphite with pore sizes of 1.2 nm, 2.5 nm and 5.5 nm. Taheri and Pour (2021) and Xu et al. (2022) studied the adsorption and diffusion behaviors of methane on different graphene based surfaces by both MD and GCMC methods. Whereas, Cengiz et al. (2021) examined the adsorption of methane in fullerene pillared graphene nanocomposites using only GCMC method. In a recent study by Cheng et al. (2021), the displacement of methane by carbon dioxide in nanoslits was explored using the MD method.

Molecular simulations by the MD and GCMC methods

(Frenkel and Smit, 2001) are useful tools to investigate shale gas adsorption and to understand the adsorption mechanisms at the detailed microscopic level. It is more cost-effective than conducting experiments physically. Moreover, factors such as temperature, pressure, and different molecules can be investigated. Newton’s equations of motion are used in the MD method to show the evolution of particles over time. In MD simulations, the positions (coordinates and orientations) and velocities (linear and angular) of the particles are calculated for every step. In the GCMC method, particles are moved randomly and the real trajectories of the system cannot be generated, meaning the system does not develop along a physical path. In both methods, the interactions between atoms are calculated using the forcefield, which collects all the atomic parameters and functions necessary for this calculation. In MD the forces of each atom are computed in parallel, while in GCMC only one particle is moved at a time. The advantage of the GCMC method, is that it directly gives the number of molecules adsorbed in the pore and shows the variation of adsorption amount by pressure. Since the MD method is good for modeling molecular motions and obtaining dynamic information about the system, and the GCMC method is good for calculating the thermodynamic parameters of the system, these two methods can be applied together to get a broader understanding of the system (Kowalczyk et al., 2005; Chen et al., 2017; Gowers et al., 2018).

2. Simulation model and methods

2.1 GCMC simulations

2.1.1 Model and simulation details

In constructing the model, the built-in graphene structure in Materials Studio 7.0 was used. The original cell lattice constant is as follows, $a = 2.46$ Å, $b = 4.26$ Å, $c = 30$ Å, $\alpha = \beta = \gamma = 90^\circ$. The nanoslit was created using the $24a \times 5b$ supercell, which created the size in the $x \times y$ directions of 59.03 Å \times 21.3 Å. The slit pore size in the z direction was determined by different H values (0.85 nm, 1.00 nm, 1.50 nm and 2.00 nm). To ensure periodicity, the model was constructed in the form of a periodic rectangle with a slit pore width H and a space above and below it with a height of $H/2$ as shown in Fig. 1.

The simulation of the adsorption isotherm was conducted using the GCMC method. The Metropolis sampling method was used to obtain a sequence of random samples and production steps of 100,000 and equilibration steps of 10,000 were used to ensure good quality. The forcefield used for the simulations is condensed-phase optimized molecular potentials for atomistic simulation studies II (COMPASS II) with forcefield-assigned charges. The Ewald method was used to calculate the electrostatic force, and the atom-based method was used to calculate the van der Waals force with the cutoff distance of 12.5 Å. To make the model similar to the shale reservoir, the temperature was set as 318 K, and the pressure range of 0 to 40 MPa was used. The GCMC simulations on all pore sizes were conducted with CH_4 , CO_2 , and N_2 molecules. The unit of the adsorption amounts obtained from simulations

is molecules per unit cell. To compare the adsorption of molecules with other similar studies and experiments, it is converted to millimoles of a molecule per gram of graphene (mmol/g).

To determine the dependence of adsorption amount on forcefields, the GCMC simulations for methane in a 1 nm pore at a temperature of 298 K were conducted for the COMPASS, COMPASS II, consistent valence forcefield (CVFF), and polymer consistent forcefield (PCFF) forcefield models. Finally, the effect of different temperatures on adsorption amounts was analyzed. The GCMC simulations of methane molecule for the pore size of 1 nm were conducted with the temperatures of 273 K, 283 K, 293 K, 303 K, 313 K, and 333 K using the COMPASS II forcefield.

2.1.2 Adsorption isotherms

Adsorption isotherm is one of the most important aspects of understanding the adsorption process. It is useful in optimizing the adsorption process, describing the properties of adsorbents and in designing the adsorption setup (Foo and Hameed, 2010). Adsorption isotherm is described as the total amount of gas molecules present in the pore space as a function of pressure at a constant temperature. It includes both the gas molecules adsorbed on the surface of the graphene walls as well as the molecules in the central space of the pore (Mosher et al., 2013).

An adsorption model is essential for describing the adsorption process and determining the maximum adsorption amount. For this reason, numerous adsorption models, that are based on various theories, including mono-layer adsorption, multi-layer adsorption and micropore filling, have been developed over the years (Zhou et al., 2022). The data obtained from molecular simulations were fitted with two commonly used isotherm models, Langmuir and Freundlich. In order to find the adsorption model that best describes the adsorption of gas molecules on a graphene surface, the coefficient of regression, R^2 , is used.

In this work, adsorption isotherms were analyzed using the Langmuir model and the Freundlich model, both commonly used in the analysis of gas adsorption (Foo and Hameed, 2010; Ammendola et al., 2017). The Langmuir equation is:

$$q_e = \frac{q_s K_L P}{1 + K_L P} \quad (1)$$

where q_e is the adsorption amount in mmol/g, q_s is the maximum adsorption amount in mmol/g, K_L is the adsorption constant in MPa^{-1} , P is the equilibrium pressure in MPa. The Freundlich equation is:

$$q_e = k_F P^{1/n} \quad (2)$$

where k_F is the isotherm constant in $\text{mmol} \cdot \text{MPa}^{-1/n} / \text{g}$ and n is the heterogeneity factor that represents a deviation from the linearity of adsorption, and is also known as the Freundlich coefficient.

2.1.3 Excess adsorption and isosteric heat

Excess adsorption is described as the extra amount of gas molecules that are absorbed in comparison to the amount of

gas that would be present in the same pore volume in the absence of pore walls (Mosher et al., 2013). According to Mosher et al. (2013) the extra gas density in the system as a result of adsorption is calculated by deducting the expected gas density in the volume from the total adsorption since the gas in the adsorbed phase has a higher density than the same gas in the bulk phase. Thus, the excess adsorption amount (n_{ex} , mmol/g) can be calculated by:

$$n_{ex} = N - \frac{\rho_g V_p}{M} \quad (3)$$

where N is the total amount of gas in mmol/g, ρ_g is the equilibrium density of the gas in g/cm^3 , V_p is the free volume in the pore in cm^3/g , and M is the molar mass in unit of g/mmol. The free volume was determined using the method proposed by Talu and Myers (2001). They used helium as a reference gas, assuming it is not adsorbed to the walls (Busch and Gensterblum, 2011). The equilibrium densities for all the gases were calculated using the Soave-Redlich-Kwong equation of state (Soave, 1972).

Another important quantity used to study the adsorption process is the heat of adsorption, which is the energy released when molecules transfer from bulk to adsorbed state (Hlushak, 2018). It represents the strength of attraction of the adsorbate into the solid adsorbent surface (Abdulsalam et al., 2020). Depending on the strength of the interaction between the adsorbate and adsorbent, the adsorption process is subdivided into chemisorption and physisorption (Sims et al., 2019). All weak electrostatic interactions, such as dipole-dipole and London forces, as well as van der Waals interactions, are collectively referred to as physisorption (Sims et al., 2019). Chemisorption, on the other hand, occurs when the covalent bond between the adsorbate and adsorbent is formed as a result of electron sharing or transferring (Sims et al., 2019). Chemisorption mainly involves monolayer surface coverage, while physisorption can entail either monolayer or multilayer surface coverage (Busch and Gensterblum, 2011).

The isosteric heat of adsorption Q_{st} (kcal/mol) at a given loading is obtained from the Clapeyron equation:

$$Q_{st} = RT \frac{d(\ln p)}{d(\ln T)} \quad (4)$$

where p is the pressure value in kPa, T is the temperature value in K, R is the universal gas constant ($8.314 \text{ J}/(\text{K} \cdot \text{mol})$). Similarly, other studies used the Clausius-Clapeyron equation to calculate the isosteric heat from adsorption isotherms (Hsu et al., 2010; Yuan et al., 2013). For simplicity in comparing the isosteric heats with other studies, it is converted to kJ/mol and plotted against loading in (mmol/g).

2.2 MD simulations

Complex structures of nanoslits in shales were modeled, as slit pores, consisting of two disconnected and fixed graphite plates saturated with hydrogen atoms at the edges (see Fig. 2). The interlayer distances of 6 Å, 7 Å, 10 Å, 15 Å, and 20 Å were selected to investigate the effect of slit pore width on the methane adsorption. In constructing the model, the built-in graphene structure in Materials Studio 7.0 was used. It was

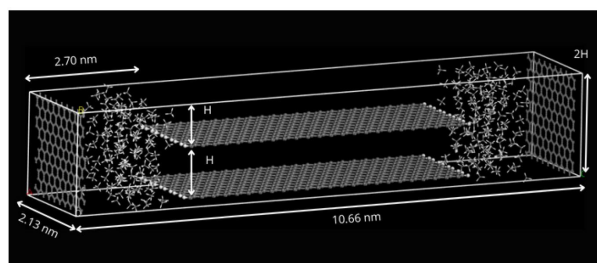


Fig. 2. Illustration of a representative adsorption model with periodic boundary conditions used in MD simulations.

given as a supercell with triclinic lattice type and dimensions of $a = 2.46 \text{ \AA}$, $b = 4.26 \text{ \AA}$, $c = 30 \text{ \AA}$, $\alpha = \beta = \gamma = 90^\circ$. CH_4 , CO_2 and N_2 gas molecules were constructed by sketching atoms. All three molecules and the graphene layer were optimized geometrically using the COMPASS II forcefield.

The bulk phase of methane was prepared with a vertical graphene layer on one side and connected to a slit pore on the other side to simulate methane adsorption. The amorphous cell was constructed in such a way that the lengths of a and b were equal to the width and height of the box, respectively. 2.13 nm for the a value, and depending on the slit pore size the b value was selected as 1.2 nm, 1.4 nm, 2.0 nm, 3.0 nm and 4.0 nm. The amount of methane in the bulk phase was set based on the density of the amorphous cell which was equal to 0.657 g/cm^3 to obtain approximately the same pressure. A representative adsorption model used in MD simulations is shown in Fig. 2. Under the pressure of the bulk phase of methane, due to the attraction potentials, methane molecules enter the slit pore and start to adsorb on the walls. The simulations were conducted in the canonical ensemble with a total simulation time of 2 ns. The temperature is controlled by a Nosé-Hoover thermostat. At the same time, the influence of temperature in the range of 0 to 80°C was investigated.

To simulate the displacement process of adsorbed methane by gas injections, the slit pore after the adsorption process is connected with the bulk phase of injected gases. Due to the pressure difference, the injected gases enter the slit pore and displace adsorbed methane. Simulations were conducted in the NVT ensemble with a total simulation time of 2 ns and a sampling frequency of 0.02 ns. The temperature is controlled by a Nosé-Hoover thermostat. The influence of temperature on the density profile was investigated. Radial distribution functions (RDFs) and methane density profiles were calculated to explore the structural information (see Fig. 3) for the adsorbed CH_4 , CO_2 and N_2 in the graphene slit pore.

Simulations for a pore size of 1.5 nm at 293 K were selected as a case study to analyze the RDFs. The trajectory for the RDF analysis was selected so that the data were analyzed only after equilibration—the last 200 ps (20 frames). Sets between carbon (graphene)- CH_4 , CO_2 and N_2 were studied with a cutoff distance of 2 nm and an interval of 0.02 nm. Periodic self-interactions were included. Note that for those analyses all three molecules were introduced as particles, while carbon was selected as a distinct atom of the graphene layer.

The influence of temperature and slit pore size on methane

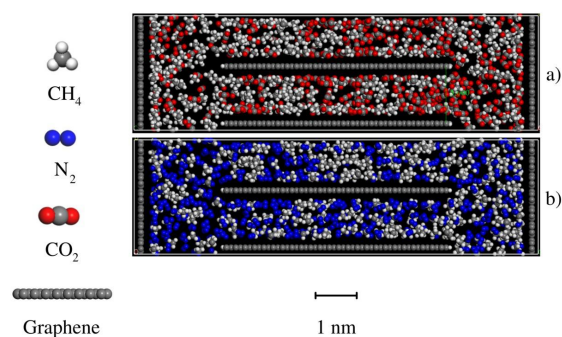


Fig. 3. Simulation snapshots by the end of the displacement of CH_4 by (a) CO_2 and (b) N_2 at a temperature of 293 K and pore size of 1.5 nm.

adsorption and its displacement by CO_2 and N_2 gases were analyzed based on the simulation snapshots of the last 200 ps. The trajectory was selected so that the data were analyzed only after the profile reached a steady result. After obtaining raw profiles, the direction of (0 1 0) was selected to get the relative concentration of the methane on the Y-axis number density by dividing each value by the volume of the cell.

To quantify the spread of data, namely the scatter of the number density values at different points along the size of the pore, the measurement of the sample standard deviation was applied. To investigate the influence of temperature on methane adsorption, the standard deviations of 21 points were examined based on a sample size of 3. Similar analyses were performed for studying adsorption isotherms of CH_4 for the pore of 1 nm and different temperatures, where 11 points were used.

3. Results and discussion

3.1 Influence of forcefield on methane adsorption

Before carrying out the main simulations, the influence of different forcefields on methane adsorption has been studied and is demonstrated in Fig. 4. The following results were obtained from these simulations: CVFF gives the largest adsorption amount, while PCFF shows the least. COMPASS and COMPASS II, more recent forcefields, demonstrate similar results, showing a slight deviation. According to Khalkhali et al. (2019), the results obtained using the COMPASS and COMPASS II forcefields are in better agreement with the experimental data. Hence, COMPASS II forcefield has been used in this study to predict the adsorption of methane.

Concerning the adsorption isotherm model, Table 1 shows that R^2 is higher for Langmuir model, meaning it is more accurate at predicting the adsorption amount. Thus, the Langmuir isotherm model is used in fitting the simulation results. Moreover, Rexer et al. (2013), Zhao et al. (2019), Zhou et al. (2019) and many other researchers have also used the Langmuir isotherm model to analyze their adsorption data.

3.2 Influence of temperature

MD method shows that in general the amount of methane molecules adsorbed by graphene decreases with increasing te-

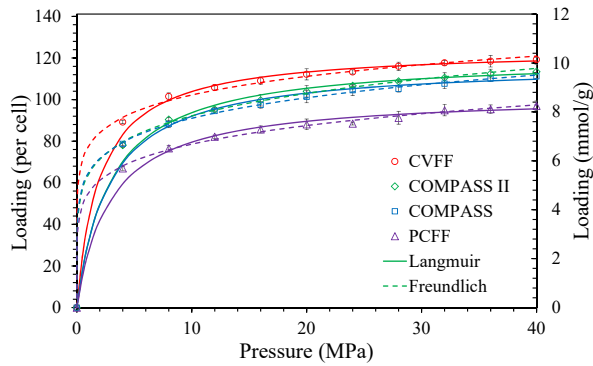


Fig. 4. Adsorption isotherms of CH₄ for the pore size of 1 nm, temperature of 298 K and different forcefields.

Table 1. Fitting parameters of the Langmuir model and Freundlich model for different forcefield models.

Parameter	CVFF	COMPASS	COMPASS II	PCFF
q_s	10.5865	9.9807	10.2515	8.7132
K_L	0.5032	0.3628	0.3489	0.3467
R^2 (Eq. (1))	0.9996	0.9986	0.9991	0.9981
n	8.2544	6.7383	6.2673	6.4320
k_F	6.5762	5.4992	5.4290	4.6707
R^2 (Eq. (2))	0.9783	0.9961	0.9917	0.9882

perature (see Fig. 5). Gao et al. (2020) stated that at high temperatures the pore structure of the graphene layers will alter and experience a blocking effect on the pore throat. Consequently, methane molecules cannot be adsorbed freely. Moreover, when the temperature increases further the desorption process occurs. Fig. 5 illustrates that at 273 K the number density profile of methane is higher than at higher temperature values, which agrees with other studies (Liu et al., 2018). The increase in the temperature causes the complex interaction between matrix swelling and shrinkage, and generation of micro-fractures, which leads to the changes in coal structure and permeability, hence the adsorption capacity decreases (Huang et al., 2011; Zou et al., 2017; Li et al., 2018; Liu et al., 2018).

Similarly, the dependence of methane adsorption on temperature was analyzed using the GCMC method. It is obvious that with the increase in temperature, the loading amount of methane decreases as shown in Fig. 6. According to Xiong et al. (2017) the mean kinetic energy of molecules increases as the temperature increases. This in turn increases the chances of molecules to overcome the van der Waals attraction forces exerted by the graphene surface (Ammendola et al., 2017). Thus, increasing the temperature results in a decrease in the adsorption amount.

The same conclusion can be drawn from the parameters of the Langmuir model. As can be seen in Table 2, both the q_s and K_L parameters decrease with increasing temperature. This trend was also observed in other similar studies (Rexer et al.,

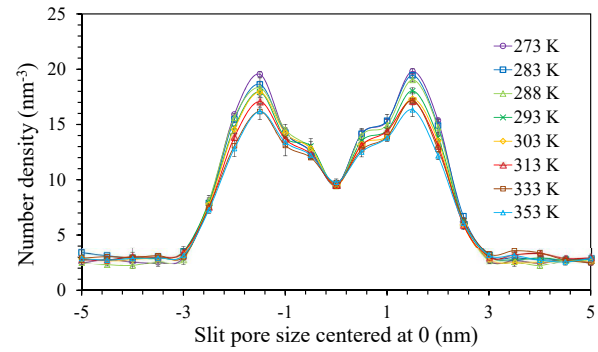


Fig. 5. Influence of temperature on methane adsorption for a slit pore of 1 nm. Error bars (\pm sample standard deviation (SD)) were included.

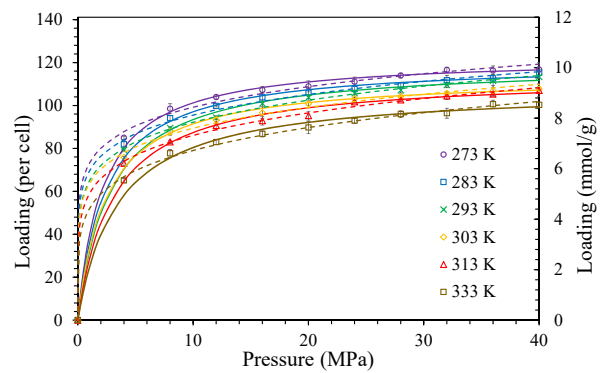


Fig. 6. Adsorption isotherms of CH₄ molecule for the pore size of 1 nm different temperatures. Error bars (\pm SD) were included. The fitting parameters are given in Table 2.

2013; Zhao et al., 2019; Zhou et al., 2019). According to Ammendola et al. (2017), the decreasing behavior of Langmuir parameters confirms that the adsorption of molecules on graphene surfaces is an exothermic process.

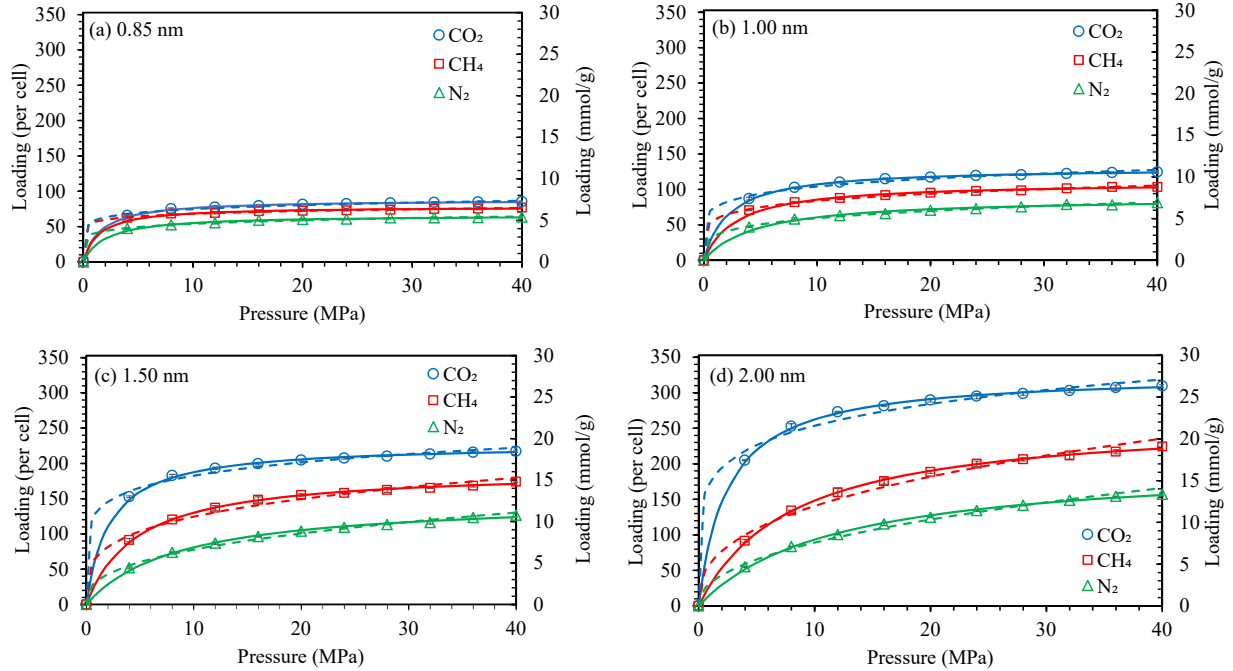
3.3 Influence of pore size

As shown by the adsorption isotherms of CH₄, CO₂, and N₂ gases in Fig. 7, adsorption amount increases with the pore size. This is because as the pore size increases, more gas molecules can penetrate the slit pore, which leads to greater adsorption. The simulations also show that the adsorption isotherms increase with pressure. This is because increasing the pressure results in more molecules striking the surface, favoring the adsorption process. Moreover, the loading of all three gases increases sharply at low pressures (0-4 MPa) and gradually slows down, which is in agreement with previous similar studies (You et al., 2016; Zhou et al., 2022). This can be explained by the fact that on a solid surface, there are a certain number of adsorption sites that can adsorb gas molecules. Thus, the number of adsorbed gas molecules increases almost linearly at the beginning. Once, all the available adsorption sites are filled, pressure no longer notably affects the adsorption (You et al., 2016).

As can be seen from Fig. 8, the excess adsorption amounts of all three gases increase with the increase in pore size, for the

Table 2. Langmuir fitting parameters of the simulation results in Fig. 6.

Parameter	T					
	273 K	283 K	293 K	303 K	313 K	333 K
q_s	10.4392	10.2108	10.1591	9.6673	9.6934	9.1744
K_L	0.4698	0.4215	0.3586	0.4102	0.3285	0.2926
R^2	0.9995	0.9991	0.9988	0.9996	0.9985	0.9981

**Fig. 7.** Adsorption isotherms of CH_4 , CO_2 and N_2 molecules for the pore sizes of (a) 0.85 nm, (b) 1.00 nm, (c) 1.50 nm and (d) 2.00 nm, and temperature of 318 K.

same reason as the increase of total adsorption amounts. With regard to the pattern of the curves, the excess adsorption of all three gases increases until reaching a maximum, at around 5-8 MPa, and decreases afterward, which is consistent with other studies (Sui et al., 2015; Zhang et al., 2015). This behavior is explained by the fact that there are many available places for adsorption at lower pressures, meaning the density of the adsorbed state increases. Once all the available adsorption sites are filled, further increase in pressure does not affect the density of adsorbed state. The density of the bulk phase, on the other hand, always increases as pressure increases. Thus, the excess adsorption, which is the difference between the adsorbed state and bulk phase densities, increases at first and decreases towards zero at higher pressures (Mosher et al., 2013). Moreover, there is a maximum excess adsorption, which means there is an optimal pressure for maximum gas storage in slit pores (Sui et al., 2015).

According to Ottiger et al. (2006), the CH_4 and N_2 excess adsorptions demonstrate a slight peak because the temperature in the shale exceeds their critical temperatures of -82.6 and -147 °C (Green and Perry, 2008), respectively. However, a distinctive trend can be observed for carbon dioxide, since its

critical temperature, 31.2 °C (Green and Perry, 2008), is close to the temperature in the shale. Its adsorption increases sharply at low pressures and decreases after reaching a maximum in the 5 to 8 MPa pressure range. An increase at the beginning is explained by a significant increase in the density of carbon dioxide when its phase changes from gaseous to supercritical state (Weniger et al., 2010). Similar to CH_4 and N_2 , the subsequent decrease in excess adsorption quantity is due to the filling up of the pores. The same tendency of carbon dioxide adsorption was observed in other studies (Ottiger et al., 2006; Busch et al., 2008; Weniger et al., 2010; Mery and Sinayuc, 2016; Liu et al., 2019).

The isosteric heat of all three gases decreases with the increase in pore size, as shown in Fig. 9. This is because, at narrow pores (0.85 nm), only one layer of fluid is formed, which can directly interact with the graphene surface (Hlushak, 2018). When the pore is wide enough for the formation of two (1.00 nm) or three (1.50 nm) fluid layers, the solid-fluid interaction becomes weaker, resulting in a decrease of the isosteric heat (Hlushak, 2018). At larger pore sizes (≥ 2.00 nm) more than three fluid layers are formed, and the direct interaction of the fluid with the surface is not

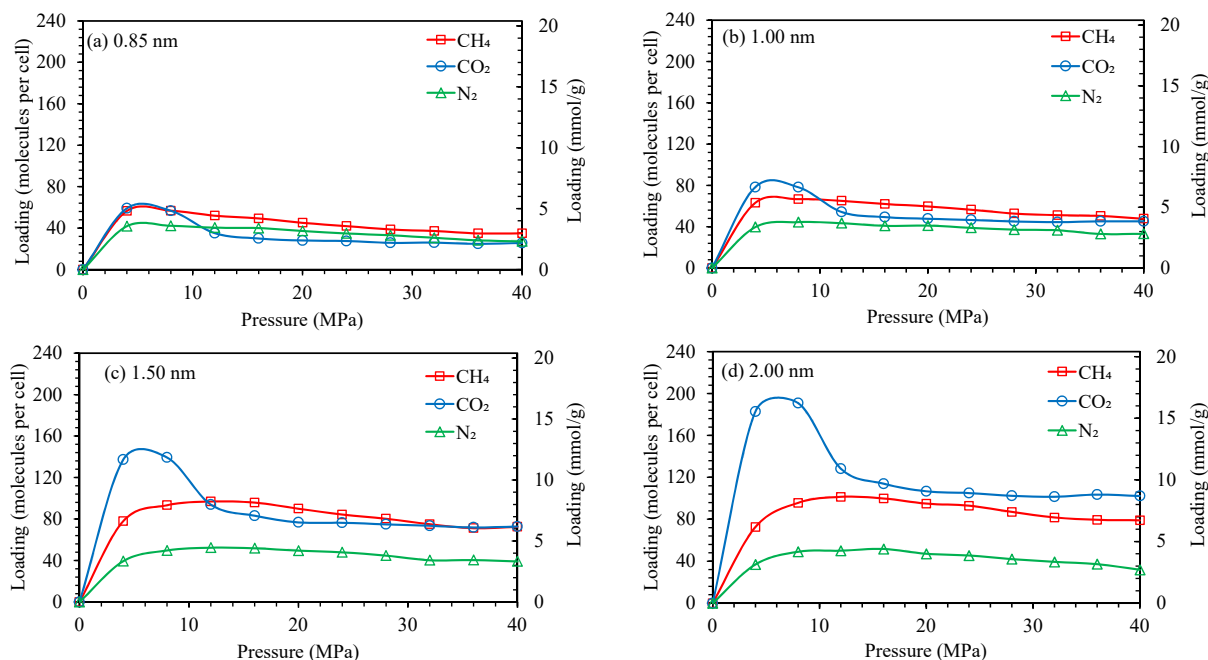


Fig. 8. Excess adsorption isotherms of CH₄, CO₂ and N₂ molecules for the pore sizes of (a) 0.85 nm, (b) 1.00 nm, (c) 1.50 nm and (d) 2.00 nm, and temperature of 318 K.

possible (Hlushak, 2018). It is also noted that the isosteric heats of all three gases increase with the increase in loading amount. According to several studies, the upward trend is attributed to an increase in the mutual attraction between adsorbate molecules with the increase of loading (Yuan et al., 2013; Hlushak, 2018; Zhou et al., 2019). Moreover, the increasing behavior of the isosteric heat with loading indicates the homogeneity of the graphene surface (Yuan et al., 2013). However, CO₂ experienced a sharper increase in isosteric heat than CH₄ and N₂. This can be attributed to the fact that CO₂ molecules are more attracted to each other than to the carbon surface (Krungleviciute et al., 2012). Finally, the isosteric heat of CO₂ is significantly higher than the isosteric heat of CH₄ and N₂. This tendency signifies the stronger interaction of the adsorbent surface with CO₂ molecules than CH₄ or N₂ (You et al., 2016). According to Abdulsalam et al. (2020), the chemisorption process is indicated by the heat of adsorption being at least 80 kJ/mol. The isosteric heats of adsorption, in Fig. 9, obtained for different pore sizes are in the range of 12-24 kJ/mol for CH₄, 9-19 kJ/mol for N₂ and 30-50 kJ/mol for CO₂. These values are significantly less than that for chemisorption, meaning the adsorption of gas molecules on the graphene surface is physisorption. This finding agrees with other similar studies (Zhou et al., 2019; Abdulsalam et al., 2020).

To investigate the effect of the pore size on adsorption and study the adsorption structures, the number density distribution profiles of methane in different slit pores (0.6 nm, 0.7 nm, 1.0 nm, 1.5 nm and 2.0 nm) were calculated and are shown in Fig. 10. The results agree with the simulation snapshots shown in Fig. 11. As is shown in Fig. 10, the minimum slit pore width at which methane molecules can penetrate the slit

pore is 0.7 nm. With interlayer widths of 0.6 nm, the methane molecules cannot penetrate the slit pore (see Fig. 11(a)) since the radius of the methane, considering it as a spherical particle, is 0.38 nm (Mohamad et al., 2016) and adding 0.25 nm of the interlamellar distance between methane and graphene molecules (Yang et al., 2018) gives 0.63 nm which is bigger than 0.6 nm. At an interlayer width of 0.7 nm, the methane molecules create a single adsorption layer in the center of the pore (Fig. 11(b)). Two or more symmetrical peaks might occur due to the separation of the attractive potentials from the two walls by increasing pore size. At an interlayer width of 1 nm, the methane molecules create two adsorption layers with the lower peaks of the number density distribution (Fig. 11(c)). For a slit pore size of 1.5 nm, the methane molecules create three adsorption layers (Fig. 11(d)). Note that the central peak has a much lower intensity than the main peaks at the edges. Finally, at an interlayer width of 2 nm, there are five adsorption layers (Fig. 11(e)). The central layer has the lowest intensity, which could be neglected.

3.4 Displacement of adsorbed methane

Displacement of loaded methane by CO₂ molecules starts from the adsorption of the CO₂ molecules on the vacancies. Since the adsorption capacity of CO₂ is stronger than the CH₄, CO₂ molecules might replace the adsorbed CH₄. Consequently, the adsorbed methane molecules get dislodged from the graphene layers and return to the free phase. Shi et al. (2019), indicated that since the most probable interaction energy for methane is around -4.5 to -2.5 kJ/mol and CH₄ CO₂ is about -8.3 to -5.1 kJ/mol, methane should be at the higher energy adsorption site, while CO₂ is at the lower energy adsorption site. In other words, the adsorption capacity of CH₄

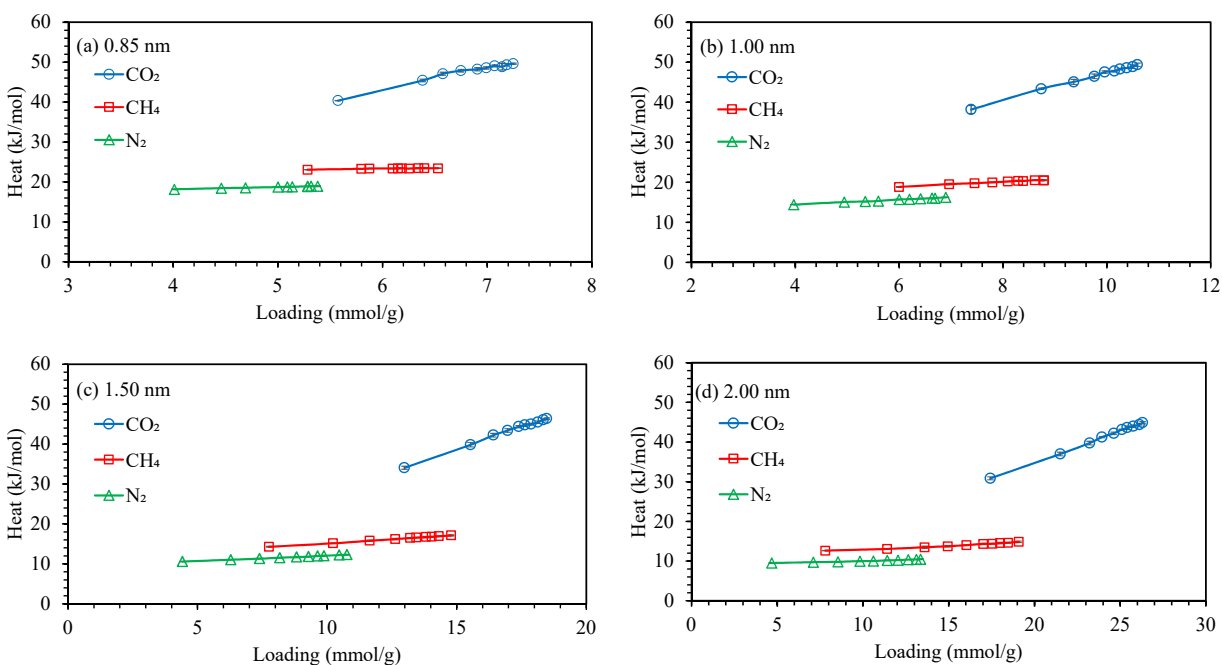


Fig. 9. Isothermic heats of adsorption of CH_4 , CO_2 and N_2 molecules for the pore sizes of (a) 0.85 nm, (b) 1.00 nm, (c) 1.50 nm and (d) 2.00 nm, and temperature of 318 K.

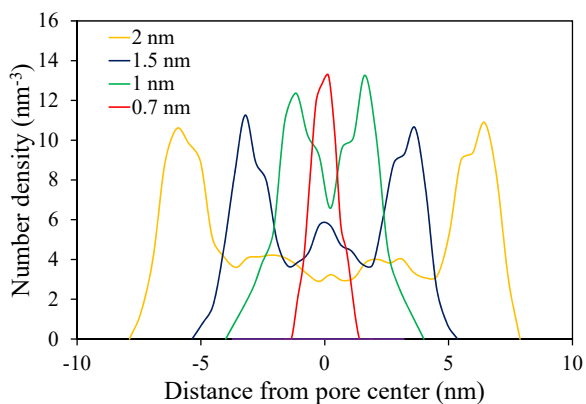


Fig. 10. Number density profiles of CH_4 in different slit pores (0.6 nm, 0.7 nm, 1.0 nm, 1.5 nm and 2.0 nm) based on the distance from the pore center at a temperature of 293 K.

is weaker than that of CO_2 . In the case of N_2 , the adsorption capacity of CH_4 is stronger than that of N_2 , therefore the N_2 molecules can only adsorb on the vacancies and substitution does not occur. However, the N_2 molecules might cause desorption and displacement of the CH_4 molecules since N_2 can isobarically decrease the partial pressure of CH_4 (Wu et al., 2015). Moreover, the displacement efficiency demonstrated a downward trend with the increase in temperature: with increasing temperature the number density profiles of CO_2 and N_2 started to behave similarly.

In experimental studies by Zhu et al. (2003) and Turt et al. (2008), it was found that CO_2 propagates through coal at constant velocity, while N_2 moves more rapidly. The obtained results in Fig. 12 strongly correlate with those studies. In general, both gases could displace the adsorbed methane effi-

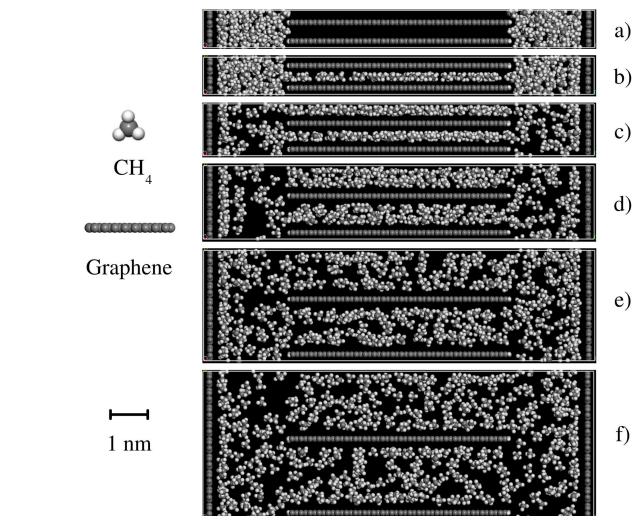


Fig. 11. Snapshots for 3D models of methane adsorption in slit pores with different interlayer distances: (a) 0.5 nm, (b) 0.6 nm, (c) 0.7 nm, (d) 1.0 nm, (e) 1.5 nm and (f) 2.0 nm at a temperature of 293 K.

ently. However, injecting CO_2 molecules results in a relatively slow breakthrough time and a sharp front. In contrast, a relatively fast breakthrough time and a wide front are observed while injecting N_2 molecules (Fig. 12). This can be explained by the fact that CO_2 travels slowly through the pore since it gets adsorbed. In the case of N_2 , it travels quickly through the pore since it is less strongly adsorbed than CH_4 . While CO_2 breaks through, the concentration of CH_4 decreases gradually. Similar results on the displacement process were also obtained by Wu et al. (2015) using a coarse-grained unitedatom model.

The RDFs $g(r)$ between CH_4 , CO_2 , N_2 and graphene (C)

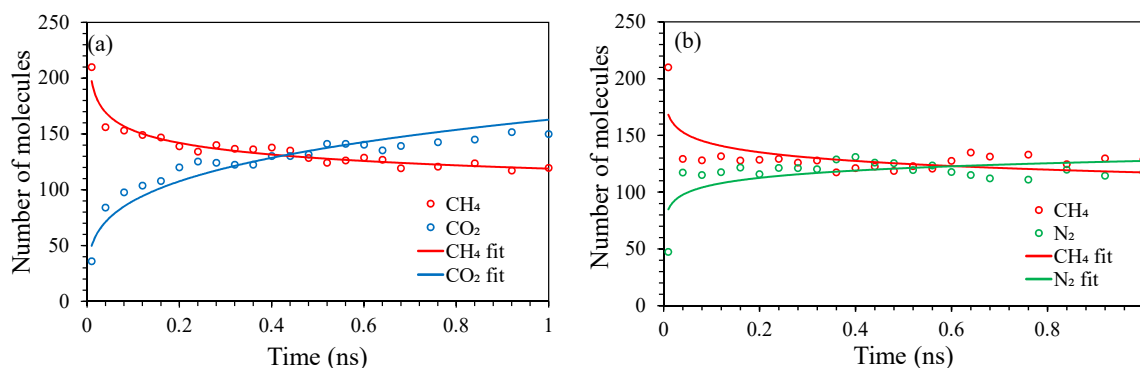


Fig. 12. Evolution of the composition profiles of CH₄ displacement by (a) CO₂ and N₂ at a temperature of 293 K and pore size of 1.5 nm.

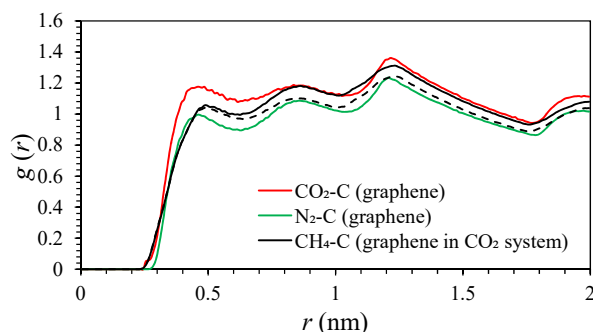


Fig. 13. RDFs between carbon atoms of graphene and CH₄, CO₂ and N₂ gas molecules at a temperature of 293 K and pore size of 1.5 nm.

are shown in Fig. 13. For CO₂ and graphene layer, there is a distinct peak at $r \approx 1.2$ nm and relatively weaker peaks at $r \approx 0.45$ and 0.85 nm. The same tendency is observed for CH₄ but with lower intensity. In the case of N₂, the same peaks are observable, however, the intensity of the RDF curve of N₂ is lower than that of CH₄ which indicates that the arrangement of CO₂ molecules in the pores is more compact than that of N₂.

Fig. 14 presents the number density profiles of methane molecules at different temperatures. It is found that the injection of gases such as CO₂ and N₂ decreases the absorption of CH₄, and at all temperature values, the number density of methane after gas injections is much lower than in the absence of gas injection. Recall that the adsorption capacity of the three gases decreases in the order of CO₂, CH₄ and N₂ (see Fig. 7). With a higher adsorption capacity, CO₂ molecules displace methane molecules and get adsorbed more intensively than N₂ molecules. This is the primary reason why ESGR, which could be performed by injection of CO₂, plays a vital role in the understanding of CO₂ sequestration. By comparing the adsorption isotherms of three gases in Fig. 7, for all the pore sizes, the value of N₂ adsorption is the smallest, and CO₂ adsorption is the greatest. This trend can be explained by the fact that the diameter of CO₂ molecules (0.33 nm) is less than

that of CH₄ (0.38 nm) and N₂ (0.36 nm) molecules (Shieh and Chung, 1999), meaning more CO₂ molecules can enter the pore than CH₄ and N₂ molecules.

4. Conclusions

The mechanisms of methane adsorption and displacement in slit pores are studied and identified using all-atom molecular dynamics and grand canonical Monte Carlo simulations. A comparison of the adsorption isotherms obtained from four different forcefield models (CVFF, PCFF, COMPASS, and COMPASS II) shows that while the results are qualitatively similar, the amount of adsorption at the same temperature, pressure, and pore width condition follows that PCFF < COMPASS ~ COMPASS II < CVFF. Because COMPASS and COMPASS II are relatively new forcefield models and are in better agreement with the experimental data, they were used in this study for further simulations.

The minimum slit pore size at which CH₄ molecules can penetrate the pore is found to be approximately 0.7 nm. As expected, with the increase of the slit pore width, the adsorption amount increases, and the adsorption structure of methane transitions from a single adsorption layer to multiple adsorption layers. In addition, the number of adsorbed molecules increases with increasing pressure or decreasing temperature.

It also confirms that the adsorption capacity of three gases decreases in the order of CO₂, CH₄ and N₂, meaning CO₂ can directly replace CH₄. Although the adsorption capacity of N₂ is lower, it can still replace CH₄ by decreasing its partial pressure. Thus, it is concluded that both of the two gases can displace the adsorbed methane efficiently.

This study provides a detailed, microscopic understanding of the competitive adsorption mechanisms of CH₄, CO₂, and N₂ in organic nanopores common in shale gas and coalbed methane reservoirs. For future studies, several topics need to be discussed and analyzed. For instance, in this work shale and coal rock minerals were simplified as graphene. However, it is necessary to take into account the influence of other functional

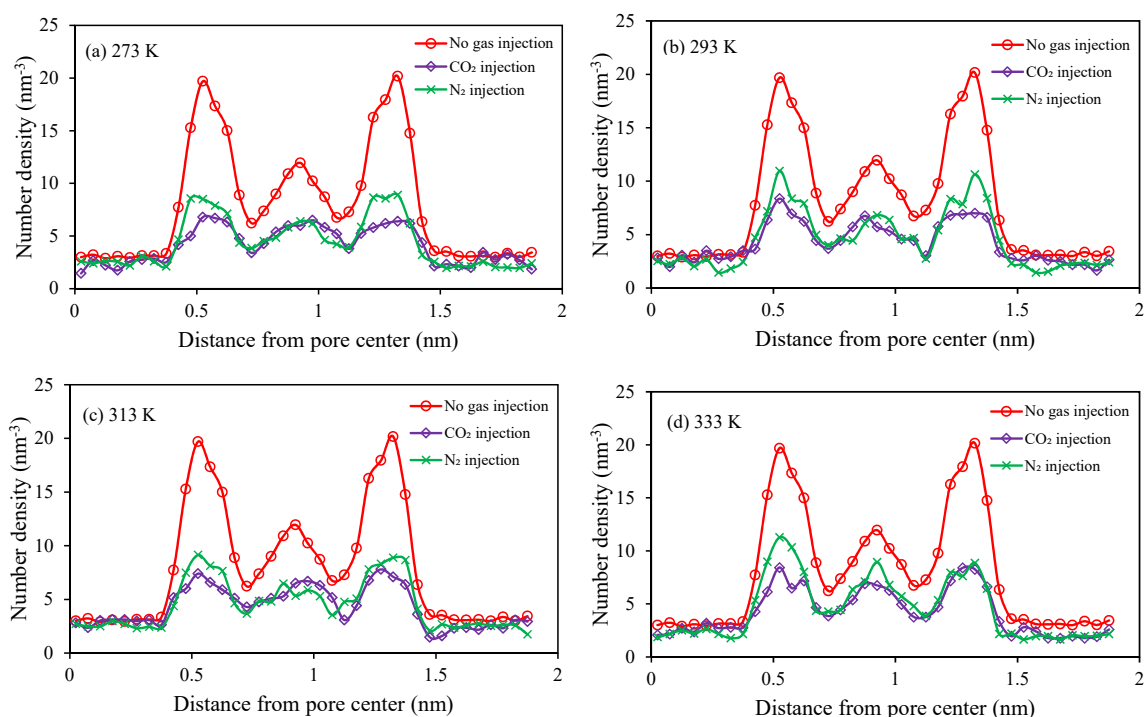


Fig. 14. Number density profiles of CH₄ molecules for the pore size of 1.5 nm after injection of CO₂ and N₂ gases under different temperature values: (a) 273 K, (b) 293 K, (c) 313 K and (d) 333 K.

groups. Moreover, the effect of water and its competitive adsorption with methane on the organic pore surface need to be investigated. In addition, it is highly necessary to explore the impact of gas flow at the nanoscale on methane adsorption and displacement in a broader sense.

Acknowledgements

This work was carried out with support from the “Simulation of sour gas injection EOR in tight carbonate reservoirs coupling capillarity and geomechanics” project (No. 080420FD1918), the “Development of cryogenic fracturing technology for coalbed methane production in Karaganda Coal Basin, Kazakhstan” project (No. 021220CRP2022), and the Social Policy Grant of Nazarbayev University. Lei Wang thanks the Science & Technology Department of Sichuan Province (No. 2021YJ0355) for financial support. We acknowledge the National Supercomputing Center in Shenzhen for providing the computational resources and Materials Studio (version 7.0) software.

Conflict of interest

The authors declare no competing interest.

Open Access This article is distributed under the terms and conditions of the Creative Commons Attribution (CC BY-NC-ND) license, which permits unrestricted use, distribution, and reproduction in any medium, provided the original work is properly cited.

References

Abdulsalam, J., Mulopo, J., Bada, S. O., et al. Equilibria and isosteric heat of adsorption of methane on activated

- carbons derived from South African coal discards. *ACS Omega*, 2020, 5(50): 32530-32539.
- Akkutlu, I. Y., Fathi, E. Multiscale gas transport in shales with local kerogen heterogeneities. *SPE Journal*, 2012, 17(4): 1002-1011.
- Ammendola, P., Raganati, F., Chirone, R. CO₂ adsorption on a fine activated carbon in a sound assisted fluidized bed: Thermodynamics and kinetics. *Chemical Engineering Journal*, 2017, 322: 302-313.
- Asif, M., Wang, L., Wang, R., et al. Mechanisms in CO₂-enhanced coalbed methane recovery process. *Advances in Geo-Energy Research*, 2022, 6(6): 531-534.
- Baykasoglu, C., Mert, H., Deniz, C. U. Grand canonical Monte Carlo simulations of methane adsorption in fullerene pillared graphene nanocomposites. *Journal of Molecular Graphics and Modelling*, 2021, 106: 107909.
- Becattini, V., Gabrielli, P., Antonini, C., et al. Carbon dioxide capture, transport and storage supply chains: Optimal economic and environmental performance of infrastructure rollout. *International Journal of Greenhouse Gas Control*, 2022, 117: 103635.
- Busch, A., Alles, S., Gensterblum, Y., et al. Carbon dioxide storage potential of shales. *International Journal of Greenhouse Gas Control*, 2008, 2(3): 297-308.
- Busch, A., Gensterblum, Y. CBM and CO₂-ECBM related sorption processes in coal: A review. *International Journal of Coal Geology*, 2011, 87(2): 49-71.
- Caulton, D. R., Shepson, P. B., Santoro, R. L., et al. Toward a better understanding and quantification of methane emissions from shale gas development. *Proceedings of*

- the National Academy of Sciences of the United States of America, 2014, 111(17): 6237-6242.
- Chen, G., Lu, S., Zhang, J., et al. Keys to linking GCMC simulations and shale gas adsorption experiments. *Fuel*, 2017, 199: 14-21.
- Cheng, X., Li, Z., He, Y. L. Release of methane from nanochannels through displacement using CO₂. *RSC Advances*, 2021, 11(25): 15457-15466.
- Foo, K. Y., Hameed, B. H. Insights into the modeling of adsorption isotherm systems. *Chemical Engineering Journal*, 2010, 156(1): 2-10.
- Frenkel, D., Smit, B. *Understanding Molecular Simulation: From Algorithms to Applications*. New York, USA, Academic Press, 2001.
- Gao, Z., Ma, D., Chen, Y., et al. Study for the effect of temperature on methane desorption based on thermodynamics and kinetics. *ACS Omega*, 2020, 6(1): 702-714.
- Gowers, R. J., Farmahini, A. H., Friedrich, D., et al. Automated analysis and benchmarking of GCMC simulation programs in application to gas adsorption. *Molecular Simulation*, 2018, 44(4): 309-321.
- Green, D. W., Perry, R. H. *Perry's Chemical Engineers' Handbook*. New York, USA, McGraw-Hill, 2008.
- Hlushak, S. Heat of adsorption, adsorption stress, and optimal storage of methane in slit and cylindrical carbon pores predicted by classical density functional theory. *Physical Chemistry Chemical Physics*, 2018, 20(2): 872-888.
- Hsu, S. C., Lu, C., Su, F., et al. Thermodynamics and regeneration studies of CO₂ adsorption on multiwalled carbon nanotubes. *Chemical Engineering Science*, 2010, 65(4): 1354-1364.
- Hu, X., Deng, H., Lu, C., et al. Characterization of CO₂/CH₄ competitive adsorption in various clay minerals in relation to shale gas recovery from molecular simulation. *Energy & Fuels*, 2019, 33(9): 8202-8214.
- Huai, J., Xie, Z., Li, Z., et al. Displacement behavior of methane in organic nanochannels in aqueous environment. *Capillarity*, 2020, 3(4): 56-61.
- Huang, H., Zhang, W., Liu, D., et al. Effect of temperature on gas adsorption and separation in ZIF-8: A combined experimental and molecular simulation study. *Chemical Engineering Science*, 2011, 66(23): 6297-6305.
- Kang, S. M., Fathi, E., Ambrose, R. J., et al. Carbon dioxide storage capacity of organic-rich shales. *SPE Journal*, 2011, 16(4): 742-755.
- Khalkhali, M., Ghorbani, A., Bayati, B. Study of adsorption and diffusion of methyl mercaptan and methane on FAU zeolite using molecular simulation. *Polyhedron*, 2019, 171: 403-410.
- Kowalczyk, P., Tanaka, H., Kaneko, K., et al. Grand canonical Monte Carlo simulation study of methane adsorption at an open graphite surface and in slitlike carbon pores at 273 K. *Langmuir*, 2005, 21(12): 5639-5646.
- Krungleviciute, V., Migone, A. D., Yudasaka, M., et al. CO₂ adsorption on dahlia-like carbon nanohorns: isosteric heat and surface area measurements. *The Journal of Physical Chemistry C*, 2012, 116(1): 306-310.
- Li, X., Yan, X., Kang, Y. Effect of temperature on the permeability of gas adsorbed coal under triaxial stress conditions. *Journal of Geophysics and Engineering*, 2018, 15(2): 386-396.
- Lin, K., Yuan, Q., Zhao, Y. P. Using graphene to simplify the adsorption of methane on shale in MD simulations. *Computational Materials Science*, 2017, 133: 99-107.
- Liu, J., Li, S., Wang, Y. Molecular dynamics simulation of diffusion behavior of CH₄, CO₂, and N₂ in mid-rank coal vitrinite. *Energies*, 2019, 12(19): 3744.
- Liu, Y., Zhu, Y., Liu, S., et al. Temperature effect on gas adsorption capacity in different sized pores of coal: Experiment and numerical modeling. *Journal of Petroleum Science and Engineering*, 2018, 165: 821-830.
- Loucks, R. G., Reed, R. M., Ruppel, S. C., et al. Morphology, genesis, and distribution of nanometer-scale pores in siliceous mudstones of the Mississippian Barnett Shale. *Journal of Sedimentary Research*, 2009, 79(12): 848-861.
- Lyu, Q., Tan, J., Li, L., et al. The role of supercritical carbon dioxide for recovery of shale gas and sequestration in gas shale reservoirs. *Energy & Environmental Science*, 2021, 14(8): 4203-4227.
- Merey, S., Sinayuc, C. Analysis of carbon dioxide sequestration in shale gas reservoirs by using experimental adsorption data and adsorption models. *Journal of Natural Gas Science and Engineering*, 2016, 36: 1087-1105.
- Mohamad, M. B., Fong, Y. Y., Shariff, A. Gas separation of carbon dioxide from methane using polysulfone membrane incorporated with Zeolite-T. *Procedia Engineering*, 2016, 148: 621-629.
- Mosher, K., He, J., Liu, Y., et al. Molecular simulation of methane adsorption in micro-and mesoporous carbons with applications to coal and gas shale systems. *International Journal of Coal Geology*, 2013, 109: 36-44.
- Ottiger, S., Pini, R., Storti, G., et al. Adsorption of pure carbon dioxide and methane on dry coal from the Sulcis Coal Province (SW Sardinia, Italy). *Environmental Progress*, 2006, 25(4): 355-364.
- Oudinot, A. Y., Riestenberg, D. E., Koperna, G. J. Enhanced gas recovery and CO₂ storage in coal bed methane reservoirs with N₂ co-injection. *Energy Procedia*, 2017, 114: 5356-5376.
- Qiao, L., Wang, H., Lu, S., et al. Novel self-adaptive shale gas production proxy model and its practical application. *ACS Omega*, 2022, 7(10): 8294-8305.
- Qin, X., Singh, H., Cai, J. Sorption characteristics in coal and shale: A review for enhanced methane recovery. *Capillarity*, 2022, 5(1): 1-11.
- Rexer, T. F., Benham, M. J., Aplin, A. C., et al. Methane adsorption on shale under simulated geological temperature and pressure conditions. *Energy & Fuels*, 2013, 27(6): 3099-3109.
- Sims, R. A., Harmer, S. L., Quinton, J. S. The role of physisorption and chemisorption in the oscillatory adsorption of organosilanes on aluminium oxide. *Polymers*, 2019, 11(3): 410.
- Sharma, A., Namsani, S., Singh, J. K. Molecular simulation of shale gas adsorption and diffusion in inorganic nanopores. *Molecular Simulation*, 2015, 41(5-6): 414-

- 422.
- Shi, J., Gong, L., Sun, S., et al. Competitive adsorption phenomenon in shale gas displacement processes. *RSC Advances*, 2019, 9(44): 25326-25335.
- Shieh, J. J., Chung, T. S. Gas permeability, diffusivity, and solubility of poly (4-vinylpyridine) film. *Journal of Polymer Science Part B: Polymer Physics*, 1999, 37(20): 2851-2861.
- Soave, G. Equilibrium constants from a modified Redlich-Kwong equation of state. *Chemical Engineering Science*, 1972, 27(6): 1197-1203.
- Sui, H., Yao, J., Zhang, L. Molecular simulation of shale gas adsorption and diffusion in clay nanopores. *Computation*, 2015, 3(4): 687-700.
- Taheri, Z., Pour, A. N. Studying of the adsorption and diffusion behaviors of methane on graphene oxide by molecular dynamics simulation. *Journal of Molecular Modeling*, 2021, 27(2): 59.
- Talu, O., Myers, A. L. Molecular simulation of adsorption: Gibbs dividing surface and comparison with experiment. *AIChE Journal*, 2001, 47(5): 1160-1168.
- Tinni, A., Fathi, E., Agarwal, R., et al. Shale permeability measurements on plugs and crushed samples. Paper SPE 162235 Presented at the SPE Canadian Unconventional Resources Conference, Calgary, Alberta, Canada, 30 October–10 November, 2012.
- Turta, A. T., Sim, S. S., Singhal, A. K., et al. Basic investigations on enhanced gas recovery by gas-gas displacement. *Journal of Canadian Petroleum Technology*, 2008, 47(10): PETSOC-08-10-39.
- Wang, L., Cheng, Y., Wang, Y. Laboratory study of the displacement coalbed CH₄ process and efficiency of CO₂ and N₂ injection. *The Scientific World Journal*, 2014, 2014: 242947.
- Weniger, P., Kalkreuth, W., Busch, A., et al. High-pressure methane and carbon dioxide sorption on coal and shale samples from the Paraná Basin, Brazil. *International Journal of Coal Geology*, 2010, 84(3-4): 190-205.
- Wu, H., Chen, J., Liu, H. Molecular dynamics simulations about adsorption and displacement of methane in carbon nanochannels. *The Journal of Physical Chemistry C*, 2015, 119(24): 13652-13657.
- Xiong, J., Liu, X. J., Liang, L. X., et al. Investigation of methane adsorption on chlorite by grand canonical Monte Carlo simulations. *Petroleum Science*, 2017, 14(1): 37-49.
- Xu, P., Rahmani, F., Chiew, Y. C. Adsorption and diffusion of methane and light gases in 3D nano-porous graphene sponge. *Molecular Simulation*, 2022, 48: 882-890.
- Yang, N., Yang, D., Zhang, G., et al. The effects of graphene stacking on the performance of methane sensor: A first-principles study on the adsorption, band gap and doping of graphene. *Sensors*, 2018, 18(2): 422.
- You, J., Tian, L., Zhang, C., et al. Adsorption behavior of carbon dioxide and methane in bituminous coal: A molecular simulation study. *Chinese Journal of Chemical Engineering*, 2016, 24(9): 1275-1282.
- Yuan, B., Wu, X., Chen, Y., et al. Adsorption of CO₂, CH₄, and N₂ on ordered mesoporous carbon: Approach for greenhouse gases capture and biogas upgrading. *Environmental Science & Technology*, 2013, 47(10): 5474-5480.
- Zhang, J., Liu, K., Clennell, M., et al. Molecular simulation studies of hydrocarbon and carbon dioxide adsorption on coal. *Petroleum Science*, 2015, 12(4): 692-704.
- Zhao, J., Wang, Z., Guo, P. Microscopic simulation of methane adsorption in organic matter. *Industrial & Engineering Chemistry Research*, 2019, 58(8): 3523-3530.
- Zheng, S., Yao, Y., Elsworth, D., et al. Dynamic fluid interactions during CO₂-enhanced coalbed methane and CO₂ sequestration in coal seams. Part 1: CO₂-CH₄ interactions. *Energy & Fuels*, 2020, 34(7): 8274-8282.
- Zhou, S., Wang, H., Li, B., et al. Predicting adsorbed gas capacity of deep shales under high temperature and pressure: Experiments and modeling. *Advances in Geo-Energy Research*, 2022, 6(6): 482-491.
- Zhou, S., Wang, H., Zhang, P., et al. Investigation of the isosteric heat of adsorption for supercritical methane on shale under high pressure. *Adsorption Science & Technology*, 2019, 37(7-8): 590-606.
- Zhu, J., Jessen, K., Kovscek, A. R., et al. Analytical theory of coalbed methane recovery by gas injection. *SPE Journal*, 2003, 8(4): 371-379.
- Zou, J., Rezaee, R., Liu, K. Effect of temperature on methane adsorption in shale gas reservoirs. *Energy & Fuels*, 2017, 31(11): 12081-12092.